

Double parton interactions in $\gamma + 3$ jet and $\gamma + b/c$ jet + 2 jet events in $p\bar{p}$ collisions at $\sqrt{s} = 1.96$ TeV

V.M. Abazov,³¹ B. Abbott,⁶⁷ B.S. Acharya,²⁵ M. Adams,⁴⁶ T. Adams,⁴⁴ J.P. Agnew,⁴¹ G.D. Alexeev,³¹ G. Alkhazov,³⁵ A. Alton^{a, 56} A. Askew,⁴⁴ S. Atkins,⁵⁴ K. Augsten,⁷ C. Avila,⁵ F. Badaud,¹⁰ L. Bagby,⁴⁵ B. Baldin,⁴⁵ D.V. Bandurin,⁷³ S. Banerjee,²⁵ E. Barberis,⁵⁵ P. Baringer,⁵³ J.F. Bartlett,⁴⁵ U. Bassler,¹⁵ V. Bazterra,⁴⁶ A. Bean,⁵³ M. Begalli,² L. Bellantoni,⁴⁵ S.B. Beri,²³ G. Bernardi,¹⁴ R. Bernhard,¹⁹ I. Bertram,³⁹ M. Besançon,¹⁵ R. Beuselinck,⁴⁰ P.C. Bhat,⁴⁵ S. Bhatia,⁵⁸ V. Bhatnagar,²³ G. Blazey,⁴⁷ S. Blessing,⁴⁴ K. Bloom,⁵⁹ A. Boehnlein,⁴⁵ D. Boline,⁶⁴ E.E. Boos,³³ G. Borissov,³⁹ M. Borysova^{l, 38} A. Brandt,⁷⁰ O. Brandt,²⁰ R. Brock,⁵⁷ A. Bross,⁴⁵ D. Brown,¹⁴ X.B. Bu,⁴⁵ M. Buehler,⁴⁵ V. Buescher,²¹ V. Bunichev,³³ S. Burdin^{b, 39} C.P. Buszello,³⁷ E. Camacho-Pérez,²⁸ B.C.K. Casey,⁴⁵ H. Castilla-Valdez,²⁸ S. Caughron,⁵⁷ S. Chakrabarti,⁶⁴ K.M. Chan,⁵¹ A. Chandra,⁷² E. Chapon,¹⁵ G. Chen,⁵³ S.W. Cho,²⁷ S. Choi,²⁷ B. Choudhary,²⁴ S. Cihangir,⁴⁵ D. Claes,⁵⁹ J. Clutter,⁵³ M. Cooke^{k, 45} W.E. Cooper,⁴⁵ M. Corcoran,⁷² F. Couderc,¹⁵ M.-C. Cousinou,¹² D. Cutts,⁶⁹ A. Das,⁴² G. Davies,⁴⁰ S.J. de Jong,^{29,30} E. De La Cruz-Burelo,²⁸ F. Déliot,¹⁵ R. Demina,⁶³ D. Denisov,⁴⁵ S.P. Denisov,³⁴ S. Desai,⁴⁵ C. Deterre^{c, 20} K. DeVaughan,⁵⁹ H.T. Diehl,⁴⁵ M. Diesburg,⁴⁵ P.F. Ding,⁴¹ A. Dominguez,⁵⁹ A. Dubey,²⁴ L.V. Dudko,³³ A. Duperrin,¹² S. Dutt,²³ M. Eads,⁴⁷ D. Edmunds,⁵⁷ J. Ellison,⁴³ V.D. Elvira,⁴⁵ Y. Enari,¹⁴ H. Evans,⁴⁹ V.N. Evdokimov,³⁴ L. Feng,⁴⁷ T. Ferbel,⁶³ F. Fiedler,²¹ F. Filthaut,^{29,30} W. Fisher,⁵⁷ H.E. Fisk,⁴⁵ M. Fortner,⁴⁷ H. Fox,³⁹ S. Fuess,⁴⁵ P.H. Garbincius,⁴⁵ A. Garcia-Bellido,⁶³ J.A. García-González,²⁸ V. Gavrilov,³² W. Geng,^{12,57} C.E. Gerber,⁴⁶ Y. Gershtein,⁶⁰ G. Ginther,^{45,63} G. Golovanov,³¹ P.D. Grannis,⁶⁴ S. Greder,¹⁶ H. Greenlee,⁴⁵ G. Grenier,¹⁷ Ph. Gris,¹⁰ J.-F. Grivaz,¹³ A. Grohsjean^{c, 15} S. Grünendahl,⁴⁵ M.W. Grünwald,²⁶ T. Guillemain,¹³ G. Gutierrez,⁴⁵ P. Gutierrez,⁶⁷ J. Haley,⁶⁸ L. Han,⁴ K. Harder,⁴¹ A. Harel,⁶³ J.M. Hauptman,⁵² J. Hays,⁴⁰ T. Head,⁴¹ T. Hebbeker,¹⁸ D. Hedin,⁴⁷ H. Hegab,⁶⁸ A.P. Heinson,⁴³ U. Heintz,⁶⁹ C. Hensel,¹ I. Heredia-De La Cruz^{d, 28} K. Herner,⁴⁵ G. Hesketh^{f, 41} M.D. Hildreth,⁵¹ R. Hirosky,⁷³ T. Hoang,⁴⁴ J.D. Hobbs,⁶⁴ B. Hoeneisen,⁹ J. Hogan,⁷² M. Hohlfeld,²¹ J.L. Holzbauer,⁵⁸ I. Howley,⁷⁰ Z. Hubacek,^{7,15} V. Hynek,⁷ I. Iashvili,⁶² Y. Ilchenko,⁷¹ R. Illingworth,⁴⁵ A.S. Ito,⁴⁵ S. Jabeen,⁶⁹ M. Jaffré,¹³ A. Jayasinghe,⁶⁷ M.S. Jeong,²⁷ R. Jesik,⁴⁰ P. Jiang,⁴ K. Johns,⁴² E. Johnson,⁵⁷ M. Johnson,⁴⁵ A. Jonckheere,⁴⁵ P. Jonsson,⁴⁰ J. Joshi,⁴³ A.W. Jung,⁴⁵ A. Juste,³⁶ E. Kajfasz,¹² D. Karmanov,³³ I. Katsanos,⁵⁹ R. Kehoe,⁷¹ S. Kermiche,¹² N. Khalatyan,⁴⁵ A. Khanov,⁶⁸ A. Kharchilava,⁶² Y.N. Kharzheev,³¹ I. Kiselevich,³² J.M. Kohli,²³ A.V. Kozelov,³⁴ J. Kraus,⁵⁸ A. Kumar,⁶² A. Kupco,⁸ T. Kurča,¹⁷ V.A. Kuzmin,³³ S. Lammers,⁴⁹ P. Lebrun,¹⁷ H.S. Lee,²⁷ S.W. Lee,⁵² W.M. Lee,⁴⁵ X. Lei,⁴² J. Lellouch,¹⁴ D. Li,¹⁴ H. Li,⁷³ L. Li,⁴³ Q.Z. Li,⁴⁵ J.K. Lim,²⁷ D. Lincoln,⁴⁵ J. Linnemann,⁵⁷ V.V. Lipaev,³⁴ R. Lipton,⁴⁵ H. Liu,⁷¹ Y. Liu,⁴ A. Lobodenko,³⁵ M. Lokajicek,⁸ R. Lopes de Sa,⁶⁴ R. Luna-Garcia^{g, 28} A.L. Lyon,⁴⁵ A.K.A. Maciel,¹ R. Madar,¹⁹ R. Magaña-Villalba,²⁸ S. Malik,⁵⁹ V.L. Malyshev,³¹ J. Mansour,²⁰ J. Martínez-Ortega,²⁸ R. McCarthy,⁶⁴ C.L. McGivern,⁴¹ M.M. Meijer,^{29,30} A. Melnitchouk,⁴⁵ D. Menezes,⁴⁷ P.G. Mercadante,³ M. Merkin,³³ A. Meyer,¹⁸ J. Meyer^{i, 20} F. Miconi,¹⁶ N.K. Mondal,²⁵ M. Mulhearn,⁷³ E. Nagy,¹² M. Narain,⁶⁹ R. Nayyar,⁴² H.A. Neal,⁵⁶ J.P. Negret,⁵ P. Neustroev,³⁵ H.T. Nguyen,⁷³ T. Nunnemann,²² J. Orduna,⁷² N. Osman,¹² J. Osta,⁵¹ A. Pal,⁷⁰ N. Parashar,⁵⁰ V. Parihar,⁶⁹ S.K. Park,²⁷ R. Partridge^{e, 69} N. Parua,⁴⁹ A. Patwa^{j, 65} B. Penning,⁴⁵ M. Perfilov,³³ Y. Peters,⁴¹ K. Petridis,⁴¹ G. Petrillo,⁶³ P. Pétroff,¹³ M.-A. Pleier,⁶⁵ V.M. Podstavkov,⁴⁵ A.V. Popov,³⁴ M. Prewitt,⁷² D. Price,⁴¹ N. Prokopenko,³⁴ J. Qian,⁵⁶ A. Quadt,²⁰ B. Quinn,⁵⁸ P.N. Ratoff,³⁹ I. Razumov,³⁴ I. Ripp-Baudot,¹⁶ F. Rizatdinova,⁶⁸ M. Rominsky,⁴⁵ A. Ross,³⁹ C. Royon,¹⁵ P. Rubinov,⁴⁵ R. Ruchti,⁵¹ G. Sajot,¹¹ A. Sánchez-Hernández,²⁸ M.P. Sanders,²² A.S. Santos^{h, 1} G. Savage,⁴⁵ L. Sawyer,⁵⁴ T. Scanlon,⁴⁰ R.D. Schamberger,⁶⁴ Y. Scheglov,³⁵ H. Schellman,⁴⁸ C. Schwanenberger,⁴¹ R. Schwienhorst,⁵⁷ J. Sekaric,⁵³ H. Severini,⁶⁷ E. Shabalina,²⁰ V. Shary,¹⁵ S. Shaw,⁵⁷ A.A. Shchukin,³⁴ V. Simak,⁷ N.B. Skachkov,³¹ P. Skubic,⁶⁷ P. Slattery,⁶³ D. Smirnov,⁵¹ G.R. Snow,⁵⁹ J. Snow,⁶⁶ S. Snyder,⁶⁵ S. Söldner-Rembold,⁴¹ L. Sonnenschein,¹⁸ K. Soustruznik,⁶ J. Stark,¹¹ D.A. Stoyanova,³⁴ M. Strauss,⁶⁷ L. Suter,⁴¹ P. Svoisky,⁶⁷ M. Titov,¹⁵ V.V. Tokmenin,³¹ Y.-T. Tsai,⁶³ D. Tsybychev,⁶⁴ B. Tuchming,¹⁵ C. Tully,⁶¹ L. Uvarov,³⁵ S. Uvarov,³⁵ S. Uzunyan,⁴⁷ R. Van Kooten,⁴⁹ W.M. van Leeuwen,²⁹ N. Varelas,⁴⁶ E.W. Varnes,⁴² I.A. Vasilyev,³⁴ A.Y. Verkheev,³¹ L.S. Vertogradov,³¹ M. Verzocchi,⁴⁵ M. Vesterinen,⁴¹ D. Vilanova,¹⁵ P. Vokac,⁷ H.D. Wahl,⁴⁴ M.H.L.S. Wang,⁴⁵ J. Warchol,⁵¹ G. Watts,⁷⁴ M. Wayne,⁵¹ J. Weichert,²¹ L. Welty-Rieger,⁴⁸ M.R.J. Williams,⁴⁹ G.W. Wilson,⁵³ M. Wobisch,⁵⁴ D.R. Wood,⁵⁵ T.R. Wyatt,⁴¹ Y. Xie,⁴⁵ R. Yamada,⁴⁵ S. Yang,⁴ T. Yasuda,⁴⁵ Y.A. Yatsunenko,³¹ W. Ye,⁶⁴ Z. Ye,⁴⁵ H. Yin,⁴⁵ K. Yip,⁶⁵ S.W. Youn,⁴⁵ J.M. Yu,⁵⁶

J. Zennaro,⁶² T.G. Zhao,⁴¹ B. Zhou,⁵⁶ J. Zhu,⁵⁶ M. Zielinski,⁶³ D. Zieminska,⁴⁹ and L. Zivkovic¹⁴

(The D0 Collaboration*)

¹LAFEX, Centro Brasileiro de Pesquisas Físicas, Rio de Janeiro, Brazil

²Universidade do Estado do Rio de Janeiro, Rio de Janeiro, Brazil

³Universidade Federal do ABC, Santo André, Brazil

⁴University of Science and Technology of China, Hefei, People's Republic of China

⁵Universidad de los Andes, Bogotá, Colombia

⁶Charles University, Faculty of Mathematics and Physics,

Center for Particle Physics, Prague, Czech Republic

⁷Czech Technical University in Prague, Prague, Czech Republic

⁸Institute of Physics, Academy of Sciences of the Czech Republic, Prague, Czech Republic

⁹Universidad San Francisco de Quito, Quito, Ecuador

¹⁰LPC, Université Blaise Pascal, CNRS/IN2P3, Clermont, France

¹¹LPSC, Université Joseph Fourier Grenoble 1, CNRS/IN2P3,

Institut National Polytechnique de Grenoble, Grenoble, France

¹²CPPM, Aix-Marseille Université, CNRS/IN2P3, Marseille, France

¹³LAL, Université Paris-Sud, CNRS/IN2P3, Orsay, France

¹⁴LPNHE, Universités Paris VI and VII, CNRS/IN2P3, Paris, France

¹⁵CEA, Irfu, SPP, Saclay, France

¹⁶IPHC, Université de Strasbourg, CNRS/IN2P3, Strasbourg, France

¹⁷IPNL, Université Lyon 1, CNRS/IN2P3, Villeurbanne, France and Université de Lyon, Lyon, France

¹⁸III. Physikalisches Institut A, RWTH Aachen University, Aachen, Germany

¹⁹Physikalisches Institut, Universität Freiburg, Freiburg, Germany

²⁰II. Physikalisches Institut, Georg-August-Universität Göttingen, Göttingen, Germany

²¹Institut für Physik, Universität Mainz, Mainz, Germany

²²Ludwig-Maximilians-Universität München, München, Germany

²³Panjab University, Chandigarh, India

²⁴Delhi University, Delhi, India

²⁵Tata Institute of Fundamental Research, Mumbai, India

²⁶University College Dublin, Dublin, Ireland

²⁷Korea Detector Laboratory, Korea University, Seoul, Korea

²⁸CINVESTAV, Mexico City, Mexico

²⁹Nikhef, Science Park, Amsterdam, the Netherlands

³⁰Radboud University Nijmegen, Nijmegen, the Netherlands

³¹Joint Institute for Nuclear Research, Dubna, Russia

³²Institute for Theoretical and Experimental Physics, Moscow, Russia

³³Moscow State University, Moscow, Russia

³⁴Institute for High Energy Physics, Protvino, Russia

³⁵Petersburg Nuclear Physics Institute, St. Petersburg, Russia

³⁶Institució Catalana de Recerca i Estudis Avançats (ICREA) and Institut de Física d'Altes Energies (IFAE), Barcelona, Spain

³⁷Uppsala University, Uppsala, Sweden

³⁸Taras Shevchenko National University of Kyiv, Kiev, Ukraine

³⁹Lancaster University, Lancaster LA1 4YB, United Kingdom

⁴⁰Imperial College London, London SW7 2AZ, United Kingdom

⁴¹The University of Manchester, Manchester M13 9PL, United Kingdom

⁴²University of Arizona, Tucson, Arizona 85721, USA

⁴³University of California Riverside, Riverside, California 92521, USA

⁴⁴Florida State University, Tallahassee, Florida 32306, USA

⁴⁵Fermi National Accelerator Laboratory, Batavia, Illinois 60510, USA

⁴⁶University of Illinois at Chicago, Chicago, Illinois 60607, USA

⁴⁷Northern Illinois University, DeKalb, Illinois 60115, USA

⁴⁸Northwestern University, Evanston, Illinois 60208, USA

⁴⁹Indiana University, Bloomington, Indiana 47405, USA

⁵⁰Purdue University Calumet, Hammond, Indiana 46323, USA

⁵¹University of Notre Dame, Notre Dame, Indiana 46556, USA

⁵²Iowa State University, Ames, Iowa 50011, USA

⁵³University of Kansas, Lawrence, Kansas 66045, USA

⁵⁴Louisiana Tech University, Ruston, Louisiana 71272, USA

⁵⁵Northeastern University, Boston, Massachusetts 02115, USA

⁵⁶University of Michigan, Ann Arbor, Michigan 48109, USA

⁵⁷Michigan State University, East Lansing, Michigan 48824, USA

⁵⁸University of Mississippi, University, Mississippi 38677, USA

⁵⁹University of Nebraska, Lincoln, Nebraska 68588, USA

- ⁶⁰Rutgers University, Piscataway, New Jersey 08855, USA
⁶¹Princeton University, Princeton, New Jersey 08544, USA
⁶²State University of New York, Buffalo, New York 14260, USA
⁶³University of Rochester, Rochester, New York 14627, USA
⁶⁴State University of New York, Stony Brook, New York 11794, USA
⁶⁵Brookhaven National Laboratory, Upton, New York 11973, USA
⁶⁶Langston University, Langston, Oklahoma 73050, USA
⁶⁷University of Oklahoma, Norman, Oklahoma 73019, USA
⁶⁸Oklahoma State University, Stillwater, Oklahoma 74078, USA
⁶⁹Brown University, Providence, Rhode Island 02912, USA
⁷⁰University of Texas, Arlington, Texas 76019, USA
⁷¹Southern Methodist University, Dallas, Texas 75275, USA
⁷²Rice University, Houston, Texas 77005, USA
⁷³University of Virginia, Charlottesville, Virginia 22904, USA
⁷⁴University of Washington, Seattle, Washington 98195, USA

(Dated: February 6, 2014)

We determine the fraction of events with double parton (DP) scattering in a single $p\bar{p}$ collision at $\sqrt{s} = 1.96$ TeV in samples of $\gamma + 3$ jet and $\gamma + b/c$ jet + 2 jet events collected with the D0 detector and corresponding to an integrated luminosity of about 8.7 fb^{-1} . The DP fractions and effective cross sections (σ_{eff}) are measured for both event samples using the same kinematic selections. The measured DP fractions range from 0.21 to 0.17, with effective cross sections in the $\gamma + 3$ jet and $\gamma + b/c$ jet + 2 jet samples of $\sigma_{\text{eff}}^{\text{incl}} = 12.7 \pm 0.2 \text{ (stat)} \pm 1.3 \text{ (syst) mb}$ and $\sigma_{\text{eff}}^{\text{HF}} = 14.6 \pm 0.6 \text{ (stat)} \pm 3.2 \text{ (syst) mb}$, respectively.

PACS numbers: 14.20Dh, 13.85.Qk, 12.38.Qk

I. INTRODUCTION

The study of deep inelastic hadron-hadron collisions is one of the main sources of knowledge about hadronic structure. We describe such a collision as the process in which a single parton (quark or gluon) from one nucleon undergoes a hard scattering off a single parton from the other nucleon. The other “spectator” partons, which do not take part in this hard $2 \rightarrow 2$ parton collision, contribute to the so-called “underlying event.” However, the probability of other partons in each nucleon to also undergo a hard scattering is not zero. The rate of multiple parton interactions (MPI) in $p\bar{p}$ collisions is directly related to the transverse spatial distribution of partons within the proton, and has been the subject of extensive theoretical studies (see e.g., [1–10]).

Relevant measurements have been performed by the AFS [11], UA2 [12], CDF [13, 14], D0 [15, 16], ATLAS [17], and CMS [18] collaborations. The first three measurements are based on samples of events having a

4-jet final state, while the CDF and D0 measurements in Refs. [14–16] use $\gamma + 3$ jet events produced by double parton (DP) scattering with $\gamma + \text{jet}$ and dijet final states. The $\gamma + \text{jet}$ production originates mainly via quark-gluon scattering in a Compton-like process, $qg \rightarrow q\gamma$, and an annihilation process, $q\bar{q} \rightarrow g\gamma$. As was shown experimentally in Refs. [13–16] and theoretically described in Ref. [19], the use of $\gamma + 3$ jet events leads to a greater sensitivity to the DP fraction as compared to 4-jet events mainly because of the better energy and angular resolutions for photon as compared with jets.

The total DP cross section σ_{DP} for the events caused by two parton scatterings with $\gamma + \text{jet}$ and dijet final states is defined as [15]

$$\sigma_{\text{DP}} = \frac{\sigma^{\gamma j} \sigma^{jj}}{\sigma_{\text{eff}}} . \quad (1)$$

Here, $\sigma^{\gamma j}$ (σ^{jj}) is the total $\gamma + \text{jet}$ (dijet) production cross section. The parameter σ_{eff} in Eq. 1 is related to the distance in the transverse plane between partons in the nucleon [2, 3, 5, 11–15]:

$$\sigma_{\text{eff}} = \left[\int (F(\beta))^2 d^2\beta \right]^{-1}, \quad (2)$$

where $F(\beta) = \int \rho(r)\rho(r - \beta)d^2r$ is the overlap function between the parton spatial distributions $\rho(r)$ in the nucleons colliding with impact parameter β (for example, see [5–7]). Here r is a distance from the center of the nucleon in transverse plane. The overlap function is normalized to unity, $\int F(\beta)d^2\beta = 1$. In case of a Gaussian spatial density $\rho(r)$, the overlap function $F(\beta) = (4\pi a^2)^{-1} \exp(-\beta^2/2a^2)$, and thus $\sigma_{\text{eff}} = 8\pi a^2$,

*with visitors from ^aAugustana College, Sioux Falls, SD, USA, ^bThe University of Liverpool, Liverpool, UK, ^cDESY, Hamburg, Germany, ^dUniversidad Michoacana de San Nicolas de Hidalgo, Morelia, Mexico ^eSLAC, Menlo Park, CA, USA, ^fUniversity College London, London, UK, ^gCentro de Investigacion en Computacion - IPN, Mexico City, Mexico, ^hUniversidade Estadual Paulista, São Paulo, Brazil, ⁱKarlsruher Institut für Technologie (KIT) - Steinbuch Centre for Computing (SCC), D-76128 Karlsruhe, Germany, ^jOffice of Science, U.S. Department of Energy, Washington, D.C. 20585, USA, ^kAmerican Association for the Advancement of Science, Washington, D.C. 20005, USA and ^lKiev Institute for Nuclear Research, Kiev, Ukraine

where a is the Gaussian width [7, 15]. The overlap function characterizes the transverse area occupied by the interacting partons. The larger the overlap (i.e., smaller β), the more probable it is to have one or more hard parton interactions in the colliding nucleons.

Table I summarizes the currently available measurements of the value of σ_{eff} . Within uncertainties, existing measurements of σ_{eff} for final states with jets and photons or W bosons are consistent. They are more precise than those with 4-jet final state. The dependence of σ_{eff} on \sqrt{s} is expected to be small [5].

In this paper we present the first measurement of the DP rates and σ_{eff} involving heavy flavor leading jet using the $\gamma + b/c$ jet + 2 jet final state and compare this measurement to the results obtained with $\gamma + 3$ jet events. The $\gamma + b/c$ -jet production is mainly caused by $b(c)g \rightarrow b(c)\gamma$ and $q\bar{q} \rightarrow g\gamma$ with $g \rightarrow Q\bar{Q}$, where $Q = b(c)$ [20]. Figure 1 shows the fractions of qg and gb subprocesses in events with $\gamma + \text{jet}$ and $\gamma + b$ -jet final states, calculated using default PYTHIA 6.4 [21] settings and the CTEQ 6.1L parton distribution function [22]. At $p_T^\gamma \approx 30$ GeV, Compton-like scattering dominates over the annihilation process, contributing about 85%–88% of events. Since the initial quarks in the Compton-like scattering for inclusive $\gamma + \text{jet}$ and $\gamma + b/c$ -jet production are typically light ($\approx 92\%$, according to the estimates done with PYTHIA) and b/c quarks, respectively, the difference between effective cross sections measured in the two processes should be sensitive to difference between light quark and heavy quark transverse spatial distributions (see Eq. 2).

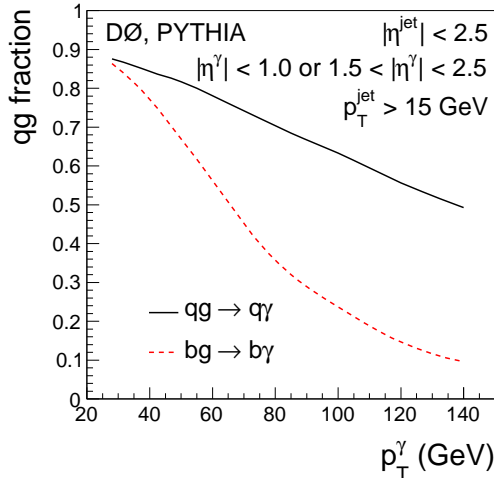


FIG. 1: (color online) Fractional contribution of the Compton-like $qg \rightarrow q\gamma$ (q is any quark type) and $bg \rightarrow b\gamma$ subprocesses to the associated production of inclusive $\gamma + \text{jet}$ and $\gamma + b$ -jet final states as a function of p_T^γ .

The outline of the paper is as follows. Section II briefly describes the technique for extracting the effective cross

section σ_{eff} . Section III includes the description of the D0 detector and the data and Monte Carlo simulation (MC) samples used in the measurement. Section IV presents signal and background models. Section V describes the discriminating variable used to determine the DP fractions. The DP fractions are estimated in Section VI. Section VII describes the determination of other parameters needed to calculate σ_{eff} . In Section VIII, we calculate the effective cross section σ_{eff} for $\gamma + 3$ jet and $\gamma + b/c$ jet + 2 jet events, and discuss the effects related to parton distribution functions (PDF) in Section IX. The results are summarized in Section X.

II. TECHNIQUE FOR EXTRACTING σ_{eff} FROM DATA

To extract σ_{eff} , we use the same technique as in earlier measurements [14, 15], which requires only quantities determined from data, minimizing the impact of theoretical assumptions. We avoid using theoretical predictions of the $\gamma + \text{jet}$ and dijet cross sections by comparing the number of $\gamma + 3$ jet events produced in DP interactions in single $p\bar{p}$ collisions to the number of $\gamma + 3$ jet events produced in two distinct hard parton interactions occurring in two separate $p\bar{p}$ collisions in the same beam crossing. The latter class of events is referred to as double interaction (DI) events. Assuming uncorrelated parton scatterings in the DP process [1–5], DP and DI events should be kinematically identical, and only differ by the presence of one (two) $p\bar{p}$ collision vertex in the case of DP (DI) events. This assumption has been tested in Ref. [15] and is discussed further in Section VIII. Both DP and DI interactions provide a source of events with two instances of parton scattering. It is necessary to measure both DP and DI rates to extract σ_{eff} . Background processes include single hard interactions producing similar final states with or without the presence of additional soft $p\bar{p}$ interactions.

As was shown in Ref. [15], the number of DI events with the final topology of interest, N_{DI} , can be obtained from the probability for a DI event, $P_{\text{DI}} = 2(\sigma^{\gamma j}/\sigma_{\text{hard}})(\sigma^{jj}/\sigma_{\text{hard}})$, in a $p\bar{p}$ beam crossing with two hard collisions. Here σ_{hard} is the total hard $p\bar{p}$ interaction cross section. This probability should be corrected for the combination of the acceptance (geometric and kinematic) and selection efficiency (ϵ_{DI}), the two-vertex event selection efficiency ($\epsilon_{2\text{vtx}}$), and the number of beam crossings with two hard collisions ($N_{2\text{coll}}$):

$$N_{\text{DI}} = P_{\text{DI}} N_{2\text{coll}} \epsilon_{\text{DI}} \epsilon_{2\text{vtx}}. \quad (3)$$

Analogously to N_{DI} , the number of DP events, N_{DP} , can be expressed from the probability for a DP event, $P_{\text{DP}} = (\sigma^{\gamma j}/\sigma_{\text{hard}})(\sigma^{jj}/\sigma_{\text{eff}})$, in a $p\bar{p}$ beam crossing with one hard collision. Similarly to the DI events, this probability is corrected for the combination of the acceptance (geometric and kinematic) and selection efficiency (ϵ_{DP}), the single-vertex event selection efficiency ($\epsilon_{1\text{vtx}}$), and

TABLE I: Summary of the results, experimental parameters, and event selection criteria for the double parton analyses performed by the AFS, UA2, CDF, D0, ATLAS, and CMS Collaborations (no uncertainties are available for the AFS result).

	\sqrt{s} (GeV)	final state	p_T^{cut} (GeV)	η range	σ_{eff}
AFS [11]	63	4 jets	$p_T^{\text{jet}} > 4$	$ \eta^{\text{jet}} < 1$	≈ 5 mb
UA2 [12]	630	4 jets	$p_T^{\text{jet}} > 15$	$ \eta^{\text{jet}} < 2$	> 8.3 mb (95% C.L.)
CDF [13]	1800	4 jets	$p_T^{\text{jet}} > 25$	$ \eta^{\text{jet}} < 3.5$	$12.1^{+10.7}_{-5.4}$ mb
CDF [14]	1800	$\gamma + 3$ jets	$p_T^{\text{jet}} > 6$ $p_T^{\gamma} > 16$	$ \eta^{\text{jet}} < 3.5$ $ \eta^{\gamma} < 0.9$	14.5 ± 1.7 (stat) $^{+1.7}_{-2.3}$ (syst) mb
D0 [15]	1960	$\gamma + 3$ jets	$60 < p_T^{\gamma} < 80$ $p_T^{\text{jet}} > 15$	$ \eta^{\gamma} < 1.0$ $1.5 < \eta^{\text{jet}} < 2.5$	16.4 ± 0.3 (stat) ± 2.3 (syst) mb
ATLAS [17]	7000	$W + 2$ jets	$p_T^{\text{jet}} > 20$	$ \eta^{\text{jet}} < 2.8$	15 ± 3 (stat) $^{+5}_{-3}$ (syst) mb
CMS [18]	7000	$W + 2$ jets	$p_T^{\text{jet}} > 20$	$ \eta^{\text{jet}} < 2.0$	20.7 ± 0.8 (stat) ± 6.6 (syst) mb

the number of beam crossings with one hard collision (N_{1coll}):

$$N_{\text{DP}} = P_{\text{DP}} N_{\text{1coll}} \epsilon_{\text{DP}} \epsilon_{\text{1vtx}}. \quad (4)$$

The ratio of the number of DP to DI events, $N_{\text{DP}}/N_{\text{DI}}$, allows us to obtain the expression for σ_{eff} [14, 15]:

$$\sigma_{\text{eff}} = \frac{N_{\text{DI}}}{N_{\text{DP}}} \frac{\epsilon_{\text{DP}}}{\epsilon_{\text{DI}}} R_c \sigma_{\text{hard}}, \quad (5)$$

where the factor $R_c \equiv (1/2)(N_{\text{1coll}}/N_{\text{2coll}})(\epsilon_{\text{1vtx}}/\epsilon_{\text{2vtx}})$. The cross sections $\sigma^{\gamma j}$ and σ^{jj} do not appear in this equation, and all efficiencies for DP and DI events enter only as ratios, resulting in a reduction of the correlated systematic uncertainties.

The background to DP events are single parton (SP) scatterings with the radiation of at least two hard gluons in the initial or final state, $qg \rightarrow q\gamma gg$, $q\bar{q} \rightarrow g\gamma gg$, which leads to the same $\gamma + 3$ jet signature. The fraction of DP events is determined using a variable sensitive to the kinematic configurations of the two independent scatterings of parton pairs.

The largest background to DI events is two-vertex SP events with one hard $\gamma + 3$ jet interaction occurring in one $p\bar{p}$ collision and an additional soft interaction (i.e., having no reconstructed jets) occurring at the other $p\bar{p}$ vertex.

III. D0 DETECTOR AND DATA SAMPLES

The D0 detector is described in detail in Refs. [23–25]. Photon candidates are identified as isolated clusters of energy depositions in one of three uranium and liquid argon sampling calorimeters. The central calorimeter covers the pseudorapidity [26] range $|\eta_{\text{det}}| < 1.1$, and the two end calorimeters cover up to $|\eta_{\text{det}}| \approx 4.2$. In addition, the plastic scintillator intercryostat detector covers the region $1.1 < |\eta_{\text{det}}| < 1.4$. The electromagnetic (EM) section of the calorimeter is segmented longitudinally into four layers and transversely into cells in pseudorapidity and azimuthal angle $\Delta\eta_{\text{det}} \times \Delta\phi_{\text{det}} = 0.1 \times 0.1$ (0.05×0.05 in the third layer of the EM calorimeter). The hadronic

portion of the calorimeter is located behind the EM section. The calorimeter surrounds a tracking system consisting of a silicon microstrip tracking (SMT) detector and scintillating fiber tracker, both located within a 2 T solenoidal magnetic field. The solenoid magnet is surrounded by the central preshower (CPS) detector located immediately before the calorimeter. The CPS consists of approximately one radiation length of lead absorber surrounded by three layers of scintillating strips.

The current measurement is based on 8.7 fb^{-1} of data collected after the D0 detector upgrade in 2006 [25], while the previous measurements [15, 16] were made using data collected before this upgrade.

The events used in this analysis pass triggers designed to identify high- p_T clusters in the EM calorimeter with loose shower shape requirements for photons. These triggers have $\approx 96\%$ efficiency at $p_T^{\gamma} \approx 30$ GeV and are 100% efficient for $p_T^{\gamma} > 35$ GeV.

To select photon candidates in our data samples, we use the following criteria [27, 28]: EM objects are reconstructed using a simple cone algorithm with a cone size of $\Delta\mathcal{R} = \sqrt{(\Delta\eta)^2 + (\Delta\phi)^2} = 0.2$. Regions with poor photon identification capability and degraded p_T^{γ} resolution at the boundaries between calorimeter modules and between the central and endcap calorimeters are excluded from analysis. Each photon candidate is required to deposit more than 96% of the detected energy in the EM section of the calorimeter and to be isolated in the angular region between $\Delta\mathcal{R} = 0.2$ and $\Delta\mathcal{R} = 0.4$ around the center of the cluster: $(E_{\text{tot}}^{\text{iso}} - E_{\text{core}}^{\text{iso}})/E_{\text{core}}^{\text{iso}} < 0.07$, where $E_{\text{tot}}^{\text{iso}}$ is the total (EM+hadronic) tower energy in the (η, ϕ) cone of radius $\Delta\mathcal{R} = 0.4$ and $E_{\text{core}}^{\text{iso}}$ is EM energy within a radius of $\Delta\mathcal{R} = 0.2$. Candidate EM clusters that match to a reconstructed track are excluded from the analysis. We also require the energy-weighted EM cluster width in the finely-segmented third EM layer to be consistent with that expected for a photon-initiated electromagnetic shower. In addition to the calorimeter isolation cut, we also apply a track isolation cut, requiring the scalar sum of track transverse momenta in an annulus $0.05 \leq \Delta\mathcal{R} \leq 0.4$ to be less than 1.5 GeV.

Jets are reconstructed using an iterative midpoint cone

algorithm [29] with a cone size of 0.5. Jets must satisfy quality criteria that suppress background from leptons, photons, and detector noise effects. Jet transverse momenta are corrected to the particle level [30].

To reject background from cosmic rays and $W \rightarrow e\nu$ decay [27], the missing transverse momentum in the event is required to be less than $0.7p_T^\gamma$. All photon-jet pairs must be separated by $\Delta\mathcal{R} > 0.7$ and all jet-jet pairs must be separated by $\Delta\mathcal{R} > 1.0$. Each event must contain at least one photon in the pseudorapidity region $|\eta^\gamma| < 1.0$ or $1.5 < |\eta^\gamma| < 2.5$ and at least three jets with $|\eta^{\text{jet}}| < 2.5$. The jet with the highest p_T is termed the “leading jet” or first jet, and the jets with the second and third highest p_T are denoted as the second and third jets in the following. Events are selected with photon transverse momentum $p_T^\gamma > 26$ GeV, leading jet $p_T^{\text{jet}} > 15$ GeV, while the next-to-leading (second) and third jets must have $15 < p_T^{\text{jet}} < 35$ GeV. The upper limit on the p_T of the second and third jets increases the fraction of DP events in the sample [15].

To select the sample of $\gamma + b/c$ jet + 2 jet candidate events, the leading jet is required to have at least two associated tracks with $p_T > 0.5$ GeV and each track must have at least one hit in the SMT detector. At least one track must have $p_T > 1.0$ GeV. These requirements ensure that there is sufficient information to identify the leading jet as a heavy flavor candidate and have a typical efficiency of about 90%. To enrich the sample with heavy flavor jets, a neural network based b -tagging algorithm (b -NN) [31] is used. It exploits long decay lengths of b -flavored hadrons. The leading jet is required to pass a tight b -NN cut > 0.225 [31].

Data events with a single $p\bar{p}$ collision vertex (“1VTX” sample), which contain DP candidates, are selected separately from events with two vertices (“2VTX” sample), which contain DI candidates. The collision vertices in both samples are required to have at least three associated tracks and to be within 60 cm of the center of the detector along the beam (z) axis. The total number of $\gamma + 3$ jet and $\gamma + b/c$ jet + 2 jet candidate events, referred to below as inclusive and heavy flavor (HF) samples, in each of the 1VTX or 2VTX categories after all selection criteria have been applied are given in Table II. No requirement on the origin vertex for the photon or jets is imposed here for the 2VTX events.

TABLE II: The numbers of selected 1VTX and 2VTX candidate events, $N_{1\text{vtx}}$ and $N_{2\text{vtx}}$, and their ratio in the $\gamma + 3$ jet (inclusive) and $\gamma + b/c$ jet + 2 jet (HF) samples.

Data Sample	$N_{1\text{vtx}}$	$N_{2\text{vtx}}$	$N_{2\text{vtx}}/N_{1\text{vtx}}$
Inclusive	218686	269445	1.23 ± 0.01
HF	5004	5811	1.16 ± 0.02

IV. DATA, SIGNAL, AND BACKGROUND EVENT MODELS

This section gives an overview of the DP and DI models built using data and MC samples, to estimate the number of DP and DI events in data, N_{DP} and N_{DI} . These models are also used to calculate selection efficiencies and geometric and kinematic acceptances for DP and DI events.

A. Signal models

• DP data event model (MIXDP):

The DP signal event model exploits the fact that two parton-parton scatterings can occur in the same $p\bar{p}$ collision. Therefore, an individual signal DP event is constructed by overlaying one event from an inclusive data sample of $\gamma + \geq 1$ jet data events with another event from a sample of inelastic non-diffractive events selected with a minimum bias trigger and a requirement of at least one reconstructed jet (“MB” sample) [15, 30]. Both input samples contain only events with a single $p\bar{p}$ collision vertex. The p_T values of the jets from the MB event are recalculated relative to the vertex of the $\gamma + \text{jet}$ event. The resulting mixed event is required to satisfy the same selection criteria as applied to $\gamma + 3$ jet data events with a single $p\bar{p}$ collision. The MIXDP sample provides independent parton scatterings with $\gamma + \text{jet}$ and dijet final states, by construction. In particular, since the $\gamma + \text{jet}$ process is dominated by small parton momentum fractions (x), the x values in the dijet production process remaining after the first parton interaction occurred is generally unaffected, i.e. the two interactions have negligible correlation in the momentum space. The mixing procedure is shown schematically in Fig. 2. The MIXDP events shown in Fig. 2(b) comprise about 60% of both inclusive and HF samples.

• DI data event model (MIXDI):

The DI signal event model assures that the $\gamma + 3$ jet DI events originate from two separate $p\bar{p}$ collisions by preparing a mixture of $\gamma + \geq 1$ jet events from the $\gamma + \text{jet}$ data and of MB events with requirements of ≥ 1 selected jets and two $p\bar{p}$ collision vertices for both data samples. Thus, the second $p\bar{p}$ collision contains only soft underlying energy that can contribute energy to a jet cone, or a photon isolation cone. In addition, in the case of ≥ 2 jets in either component of the MIXDI mixture (i.e., in $\gamma + \text{jet}$ or MB events), the two leading jets are required to originate from the same vertex, using jet track information, as discussed in Appendix B of Ref. [15]. Since the p_T of all reconstructed objects is calculated with respect to the primary $p\bar{p}$ collision vertex

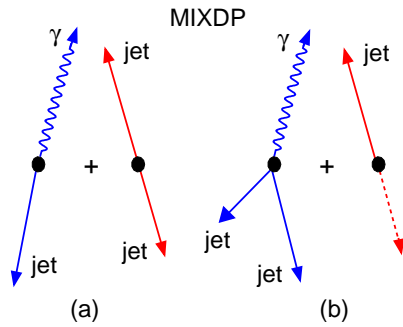


FIG. 2: (color online) Schematic view of the mixing procedure used to prepare the MIXDP signal sample. Two combinations are considered: (a) $\gamma + 1$ jet and two jets from a dijet event and (b) $\gamma + 2$ jets and one jet from a dijet event. The dotted line represents a jet failing the selection requirements since this jet is either not reconstructed or beyond kinematic selection limits.

(PV0), the jet p_T from the MB event is recalculated relative to the primary vertex of the $\gamma + \text{jet}$ event (i.e., PV0 for the 2VTX data sample). Here the PV0 is the $p\bar{p}$ collision vertex with the lowest probability that it originates from a soft $p\bar{p}$ interaction [31]. The resulting $\gamma + 3$ jet events undergo the same selection as applied to the data sample with two $p\bar{p}$ collision vertices.

A fraction of the $\gamma + 2$ jet events coming from one hard interaction in the MIXDP and MIXDI models may be caused by DP events. This fraction was measured in Ref. [16] as a function of the second jet p_T . With our current selections, we have $\langle p_T^{\text{jet}2} \rangle \approx 24$ GeV, and this fraction is expected to be around 4%–5%. Since in Eq. 5 we calculate the ratio of DP and DI events, and the fractions of the $\gamma + 2$ jet events in the MIXDP and MIXDI models are similar, it has been found that the corresponding DP fractions cancel.

To construct a model of $\gamma + b/c \text{ jet} + 2 \text{ jet}$ DP and DI signal events, the leading jet in both the MIXDP and MIXDI samples should additionally satisfy the tight b identification criteria described in the previous section.

To create signal and background MC models for DP and DI events, we use an overlay of MC $\gamma + \text{jet}$ ($\gamma + b/c \text{ jet}$) and dijet events. These events are generated with PYTHIA or SHERPA [32] event generators and processed through a GEANT-based [33] simulation of the D0 detector response. To accurately model the effects of multiple $p\bar{p}$ interactions and detector noise, data events from random $p\bar{p}$ crossings are overlaid on the MC events using data from the same data taking period as considered in the analysis. These MC events are then processed using the same reconstruction code as for data. We also apply additional smearing to the reconstructed photon and jet p_T so that the measurement resolutions in MC match those in data. These MC events are used to create single- and two-vertex samples.

- **DP and DI MC models (MCDP and MCDI):**

Using the $\gamma + \text{jet}$ ($\gamma + b/c \text{ jet}$) and dijet MC samples, we create $\gamma + 3 \text{ jet}$ ($\gamma + b/c \text{ jet} + 2 \text{ jet}$) DP and DI MC models, similar to those constructed for MIXDP and MIXDI data samples, by examining information for jets and the photon at both the reconstructed and particle level. These samples are used to calculate efficiencies and acceptances for DP and DI events. As a cross check, we have compared p_T and η distributions for the jets and the photon at the reconstruction level in these models with those in the MIXDP and MIXDI data samples. Small discrepancies have been resolved by reweighting the MC spectra and creating models denoted as data-like MCDP and MCDI.

B. Background models

To extract fractions of DP and DI events from data, we need to build SP background models.

- **SP one-vertex event model (SP1VTX):**

A background to the DP events are single parton-parton scatters with two additional bremsstrahlung jets resulting in a $\gamma + 3 \text{ jet}$ final state in a single $p\bar{p}$ collision event. To model this background, we consider a sample of MC $\gamma + 3 \text{ jet}$ events generated with MPI modeling removed. The SP1VTX sample contains the final state with a photon, leading jet, and two additional bremsstrahlung jets with the same selection criteria as applied to the data sample with a single $p\bar{p}$ collision vertex. The SHERPA SP model is taken as the default.

- **SP two-vertex event model (SP2VTX):**

The background to DI events differs from the SP1VTX model in that the $\gamma + 3 \text{ jet}$ MC events are selected with two reconstructed $p\bar{p}$ collision vertices. Events with no jet activity in the second vertex are selected by requiring the three jets to originate from the primary $p\bar{p}$ collision vertex.

To model the background to the $\gamma + b/c \text{ jet} + 2 \text{ jet}$ DP and DI processes, the SP1VTX and SP2VTX samples are constructed using the same techniques, but using $\gamma + b/c \text{ jet}$ events generated with the PYTHIA and SHERPA MCs with MPI modeling removed.

V. DISCRIMINATING VARIABLE

Unlike the SP scattering $2 \rightarrow 4$ process, which produces a $\gamma + \text{jet}$ final state and two bremsstrahlung jets, the DP mechanism has two independent $2 \rightarrow 2$ parton-parton scatterings within the same $p\bar{p}$ collision, resulting in substantially different kinematic distributions in the final state. Discrimination between these processes is obtained by examining the azimuthal angle between the p_T

vectors of two object pairs in $\gamma + 3$ jet events,

$$\Delta S \equiv \Delta\phi(\vec{P}_T^1, \vec{P}_T^2), \quad (6)$$

where $\vec{P}_T^1 = \vec{p}_T^\gamma + \vec{p}_T^{\text{jet1}}$ and $\vec{P}_T^2 = \vec{p}_T^{\text{jet2}} + \vec{p}_T^{\text{jet3}}$. Figure 3 illustrates a possible orientation of photon and jets transverse momentum vectors in $\gamma + 3$ jet events, as well as the vectors \vec{P}_T^1 and \vec{P}_T^2 .

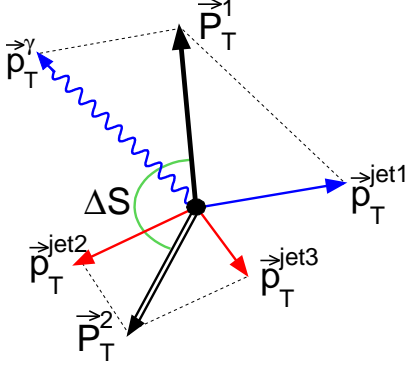


FIG. 3: (color online) A possible configuration of photon and jets transverse momenta vectors in $\gamma + 3$ jet events. Vectors \vec{P}_T^1 and \vec{P}_T^2 are the p_T -imbalance vectors of $\gamma + \text{jet}$ and dijet pairs.

The differential cross section as a function of ΔS was measured in Ref. [16] and compared with various SP and MPI models. Momentum conservation causes ΔS to peak near π , and this is particularly visible in SP, although detector resolution effects and additional gluon radiation produce a significant number of events at smaller angles. For DP events, where the photon and leading jet usually come from one parton-parton scattering and the two other jets usually come from another parton-parton scattering, the pairwise balance ΔS angle has no pronounced peak at any particular value, although some residual bias remains towards $\Delta S = \pi$ caused by the DP events shown in Fig. 2(b).

VI. FRACTIONS OF DP AND DI EVENTS

A. Fractions of DP events

To calculate σ_{eff} , we need the number of DP events (N_{DP}) in Eq. (5), given by the product of the fraction of DP events (f_{DP}) and the size of the 1VTX sample. The fraction f_{DP} is estimated in the $\gamma + 3$ jet 1VTX data sample using the DP (MIXDP) and SP (SP1VTX) models. The DP fractions (and σ_{eff}) are measured in the inclusive and HF samples separately.

The fraction f_{DP} is found using a maximum likelihood fit [34] of the ΔS distribution of the data to signal and background templates that are taken to be the shapes of the ΔS distribution in the MIXDP and SP1VTX models, respectively. Signal and background samples used as

templates, described in Section IV, satisfy all the selection criteria applied to the data sample.

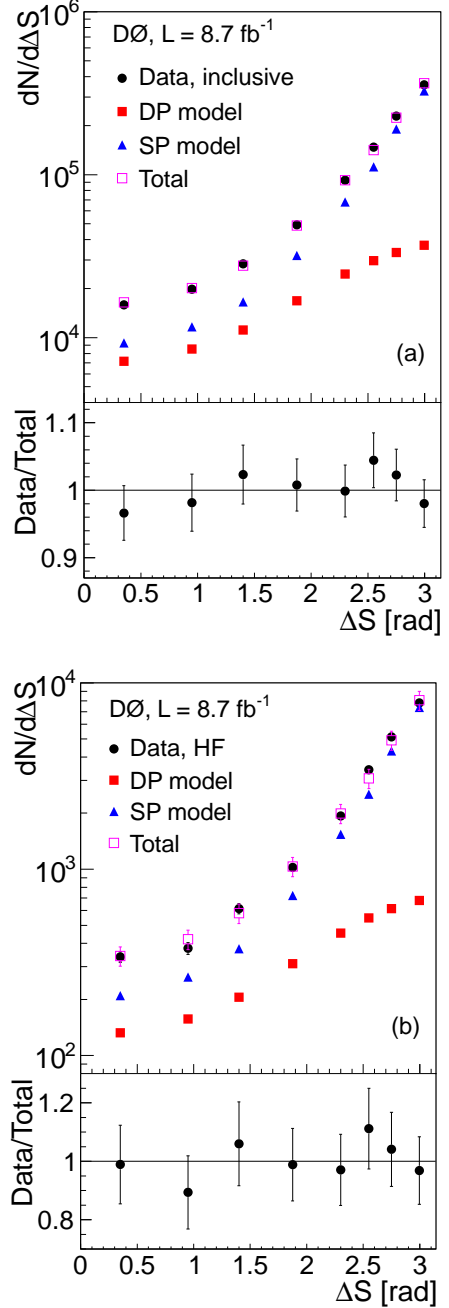


FIG. 4: (color online) The ΔS distribution in the data, DP and SP models, and the sum of the DP and SP contributions weighted with their fractions (“Total”). The plots (a) and (b) correspond to the inclusive and HF samples, respectively. The lower subplots show the relative difference of the data points with respect to the fitted sum, along with the total uncertainties, i.e. DP fraction and statistical uncertainties from data and MC added in quadrature.

A first approximation to the fractions can be obtained from the fits to inclusive and HF data shown in Fig. 4.

The measured DP fractions are:

$$f_{\text{DP}}^{\text{inc}} = 0.202 \pm 0.007 \quad (7)$$

and

$$f_{\text{DP}}^{\text{HF}} = 0.171 \pm 0.020, \quad (8)$$

respectively. If it is not stated otherwise, the uncertainties shown in Eqs. 7, 8, and in the text below are only statistical. The sum of DP and SP models weighted with their fractions describes the data with $\chi^2/ndf = 0.45$ for the inclusive case and $\chi^2/ndf = 0.26$ (with the number of degrees of freedom, $ndf = 7$) for the HF sample, i.e. $\approx 87\%$ and $\approx 97\%$ χ^2 -probability, respectively.

While the default SP model obtained with SHERPA, provides a reasonable description of the ΔS distribution in data, it might be not perfect for other related kinematic variables, which may affect the DP fractions as well. For this reason we examine two alternative models. Since the fraction of events with the leading jet coming from the second parton interaction is small ($\lesssim 10\%$), the $\Delta\phi(\gamma, \text{jet1})$ distribution (the azimuthal angle between the photon and leading jet p_T vectors) in the inclusive $\gamma + 3$ jet events should be sensitive to initial and final state radiation effects in the $\gamma + \text{jet}$ events. We construct a modified $\gamma + 3$ jet SP model in which the MC $\Delta\phi(\gamma, \text{jet1})$ distribution is reweighted to agree with data, as discussed in the Appendix. The $f_{\text{DP}}^{\text{inc,rew1}}$ fraction obtained with the $\Delta\phi(\gamma, \text{jet1})$ reweighted SP model is 0.216 ± 0.007 . The shapes of the p_T spectra of the second and third jets are important for the ΔS calculation. To estimate the effects of possible mismodeling of the jet p_T spectra, we create an alternative SP model by reweighting the jet p_T distributions in the default MC SP model in two dimensions (p_T of the second and third jet) to SP data. After reweighting, the DP fraction is recalculated and found to be $f_{\text{DP}}^{\text{inc,rew2}} = 0.195 \pm 0.007$. The sum of DP and the $\Delta\phi(\gamma, \text{jet1})$ (jet p_T) reweighted SP models weighted with their fractions describes the data with $\chi^2/ndf = 0.51$ ($\chi^2/ndf = 0.43$), $ndf = 7$.

The fraction obtained by averaging f_{DP} values after reweighting the $\Delta\phi(\gamma, \text{jet1})$ and second and third jet p_T spectra is used as a central value, and the difference between this and the value obtained with the default SP model (Eqs. 7 and 8) is taken as a systematic uncertainty. The final DP event fraction in the inclusive sample is

$$f_{\text{DP}}^{\text{inc,avg}} = 0.206 \pm 0.007 (\text{stat}) \pm 0.004 (\text{syst}). \quad (9)$$

A similar reweighting procedure and determination of central value and the assignment of uncertainties is applied for the SP model in the HF sample, and the DP fraction is found to be

$$f_{\text{DP}}^{\text{HF,avg}} = 0.173 \pm 0.020 (\text{stat}) \pm 0.002 (\text{syst}). \quad (10)$$

All the results on DP fractions are summarized in Table III.

The measured DP fraction is lower than that measured in the earlier D0 analysis [15]. This is primarily because

TABLE III: DP event fraction for different reweighting procedures.

f_{DP}	Inclusive sample	HF sample
No reweighting	0.202 ± 0.007	0.171 ± 0.020
$\Delta\phi(\gamma, \text{jet1})$ reweighted	0.216 ± 0.007	0.169 ± 0.020
p_T^{jet2} and p_T^{jet3} reweighted	0.195 ± 0.007	0.177 ± 0.020
Rewighted average	0.206 ± 0.007	0.173 ± 0.020

of the smaller jet cone radius used in the current measurement ($R = 0.5$ vs. $R = 0.7$ in [15]), what leads to a smaller probability to pass the jet reconstruction threshold (6 GeV for the uncorrected jet p_T). The use of a smaller jet cone also significantly reduces the dijet cross section (a factor of 1.5 – 2) in the p_T region of interest. Because the second parton interaction produces mostly a dijet final state, the measured DP fraction drops.

In addition to the SP events produced in single $p\bar{p}$ collisions, another source of possible background to the single-vertex $\gamma + 3$ jet DP events are two $p\bar{p}$ collisions produced very close to each other along the beam direction, so that a single vertex is reconstructed. This contribution is estimated using the instantaneous luminosity, the bunch size, the time between bunch crossings, and the vertex resolution, and found to be negligible at a level of $\lesssim 0.2\%$.

B. Fractions of DI events

In addition to f_{DP} , the fraction of DI events (f_{DI}) occurring in events with two $p\bar{p}$ collisions within the same bunch crossing must be determined to measure σ_{eff} . A discriminant is constructed using the track information of a jet and of the assignment of tracks to the two $p\bar{p}$ collision vertices (PV0 and PV1). We use the p_T -weighted position along the beam (z) axis of all tracks associated to the jet and the fraction of charged particles in the jet (CPF). The CPF discriminant is based on the fraction of total charged particles' transverse momentum (i.e., total track p_T) in each jet i originating from each identified vertex j in the event:

$$\text{CPF}(\text{jet}_i, \text{vtx}_j) = \frac{\sum_k p_T(\text{trk}_k^{\text{jet}_i}, \text{vtx}_j)}{\sum_n \sum_l p_T(\text{trk}_l^{\text{jet}_i}, \text{vtx}_n)}. \quad (11)$$

Each jet is required to have $\text{CPF} > 0.5$ and at least two tracks.

In events with two $p\bar{p}$ collisions, jets in $\gamma + 3$ jet events may originate either from PV0 or PV1. The leading jet is required to originate from PV0. Four classes of events are defined:

- I: All three jets originate from PV0.
- II: Jet 1 and jet 2 originate from PV0 while jet 3 originates from PV1.
- III: Jet 1 and jet 3 originate from PV0 while jet 2 originates from PV1.

IV: Jet 1 originates from PV0 while jet 2 and jet 3 originate from PV1.

Class I corresponds to a type of $\gamma + 3$ jet event that has all three jets originating from the same $p\bar{p}$ collision with no reconstructed jets in the other, i.e., background (non-DI) events, while classes II, III and IV correspond to three types of signal (DI) events.

To assign a jet to a vertex and extract f_{DI} using the jet track information, we need the z resolution of the jet-to-vertex assignment algorithm, σ_z . This resolution can be calculated in the $\gamma + 3$ jet data event sample with a single $p\bar{p}$ collision. Since these events have only one reconstructed $p\bar{p}$ collision vertex, all the jets should originate from this vertex. To find the z position of a jet's origin, we consider all tracks inside a jet cone and calculate the p_T -weighted position in z of all the tracks (z_{jet}). The track z position is calculated at the point of closest approach of each track to the beam axis. For each jet in the 1VTX data sample, we estimate the distance between the z_{jet} and the z -vertex position, $\Delta z(\text{vtx}, \text{jet})$. We find $\sigma_z \approx 1.2$ cm and that 98%–99% of jets in 1VTX events have $\Delta z(\text{vtx}, \text{jet}) < 3\sigma_z$. We consider a jet to originate from a vertex if $|z - z_{\text{jet}}| < 3\sigma_z$. If the jet is located within $3\sigma_z$ of both vertices it is assigned to the closest vertex.

Table IV shows the fractions of 2VTX data events in each class. From this table, one can see that the single interaction events (Class I) dominate over DI events (sum of classes II, III, and IV). The DI event fraction is $f_{\text{DI}} = 0.135 \pm 0.002$ for the inclusive sample and $f_{\text{DI}}^{\text{HF}} = 0.131 \pm 0.010$ for the sample with a heavy flavor leading jet.

TABLE IV: The fractions of 2VTX data events for Class I (non-DI events), and three classes of DI events in the $\gamma + 3$ jet (inclusive) and $\gamma + b/c$ jet + 2 jet (HF) samples.

DI event class	Inclusive sample	HF sample
I	0.865 ± 0.001	0.869 ± 0.010
II	0.074 ± 0.001	0.078 ± 0.008
III	0.044 ± 0.001	0.040 ± 0.006
IV	0.017 ± 0.001	0.013 ± 0.003

The distance in z between two vertices $\Delta z(\text{PV0}, \text{PV1})$ may affect the measured DI fraction, since about 5% of events have $\Delta z(\text{PV0}, \text{PV1}) < 3\sigma_z$. No requirement is placed on this distance in the analysis. To quantify the dependence of the DI fraction on this distance, we have also measured the DI fraction with the requirement that the two vertices are separated by $\Delta z(\text{PV0}, \text{PV1}) > 5\sigma_z$. Table V shows f_{DI} for the two cases: no cut and $\Delta z(\text{PV0}, \text{PV1}) > 5\sigma_z$. The difference between them is taken as a systematic uncertainty.

An additional uncertainty is due to the determination of the photon vertex. This uncertainty has been estimated using events with a photon EM cluster in the central region ($|\eta_{\text{det}}^\gamma| < 1.0$) with a matched CPS cluster. These events allow us to extrapolate the photon direc-

TABLE V: DI event fraction with respect to $\Delta z(\text{PV0}, \text{PV1})$.

$\Delta z(\text{PV0}, \text{PV1})$	Inclusive sample	HF sample
All values	0.135 ± 0.002	0.131 ± 0.010
$> 5\sigma_z$	0.129 ± 0.002	0.122 ± 0.011

tion along the z axis and determine the vertex position on the z axis [28]. Using the $\gamma + 3$ jet data, we estimate the photon pointing resolution in z to be about 4.5 cm. Using this resolution and the distribution of the distance in z between the first and second vertices in 2VTX events, we find that the photon origin vertex may be misidentified in about 4% of events, which is taken as a systematic uncertainty.

The DI fractions extracted for the inclusive and heavy flavor samples are:

$$f_{\text{DI}} = 0.135 \pm 0.002 (\text{stat}) \pm 0.008 (\text{syst}), \quad (12)$$

$$f_{\text{DI}}^{\text{HF}} = 0.131 \pm 0.010 (\text{stat}) \pm 0.011 (\text{syst}). \quad (13)$$

A cross check of the measured DI fractions is performed by fitting the ΔS templates for signal and background models to data as was done to extract the DP fraction in Section VIA. We use the MIXDI sample for the signal template and the SP2VTX sample for the background template (see Section IV). The measured fractions $f_{\text{DI}} = 0.127 \pm 0.021$ (with SP2VTX model taken from SHERPA) and $f_{\text{DI}} = 0.124 \pm 0.056$ (PYTHIA) are in good agreement with each other and with f_{DI} obtained by the jet-track method. The results for the heavy flavor jet sample are $f_{\text{DI}}^{\text{HF}} = 0.153 \pm 0.044$ with the SP model from SHERPA and $f_{\text{DI}}^{\text{HF}} = 0.143 \pm 0.056$ using PYTHIA, which are also in agreement with the jet-track method. Since the results of this cross check agree with the values obtained using the jet track method, we do not assign an additional systematic uncertainty.

VII. DP AND DI EFFICIENCIES, R_c AND σ_{hard}

A. Ratio of signal fractions in DP and DI events

A fraction of events with jets containing energetic π^0 or η mesons may satisfy the photon selection criteria. The photon fraction in the selected data is estimated using the maximum likelihood fit of templates from the output of the photon identification neural network (O_{NN}) in signal and background events to that in data, as described in detail in Ref. [27]. The photon fractions in DP and DI events are found to be similar. For example, for a photon in the central calorimeter (CC) region, $f_{\text{DP}}^{\gamma, \text{CC}} = 0.432 \pm 0.002$ and $f_{\text{DI}}^{\gamma, \text{CC}} = 0.437 \pm 0.004$ for DP and DI events, respectively. The photon fractions are slightly higher in the forward region due to tighter photon selections.

The fractions of events with b or c jets in the 1VTX and 2VTX data samples are estimated using templates for the

invariant mass of charged particle tracks associated with the secondary vertex, M_{SV} (see Ref. [20]) for $\gamma + b/c$ -jet and $\gamma + \text{jet}$ MC samples. The resulting HF fractions are dominated by c quarks, $f_{DP}^b = 0.352 \pm 0.025$, $f_{DP}^c = 0.551 \pm 0.041$, and $f_{DI}^b = 0.327 \pm 0.019$, $f_{DI}^c = 0.573 \pm 0.043$. The HF fractions in DP and DI samples are in good agreement. Approximately 10% of the jets tagged as HF come from mistagged light quark jets.

The overall signal fractions in DP and DI samples and their ratio in the inclusive, $f_{DP}^\gamma/f_{DI}^\gamma$, and HF samples, $(f_{DP}^\gamma f_{DP}^{\text{HF}})/(f_{DI}^\gamma f_{DI}^{\text{HF}})$, are summarized in Table VI. The systematic uncertainties on the signal fraction are caused by the uncertainties on the photon and heavy flavor fractions from O_{NN} and M_{SV} template fitting.

TABLE VI: The overall signal fractions in DP and DI samples and their ratio in the $\gamma+3$ jet (inclusive) and $\gamma+b/c$ jet + 2 jet (HF) samples. Total uncertainties are shown, i.e., statistical and systematic uncertainties added in quadrature.

Sample	DP	DI	ratio
Inclusive	0.445 ± 0.005	0.456 ± 0.008	0.976 ± 0.019
HF	0.402 ± 0.030	0.405 ± 0.030	0.993 ± 0.104

B. Ratio of signal efficiencies in DP and DI events

The selection efficiencies for DP and DI events enter Eq. (5) only as ratios, substantially canceling correlated systematic uncertainties. The DP and DI events differ from each other by the number of $p\bar{p}$ collision vertices (one vs. two), and therefore their selection efficiencies ε_{DI} and ε_{DP} may differ due to different amounts of soft unclustered energy in the single and double $p\bar{p}$ collision events. This could lead to a difference in the jet reconstruction efficiencies because of the different probabilities for jets to pass the $p_T > 6$ GeV requirement applied during jet reconstruction. It could also lead to different photon selection efficiencies because of different amounts of energy in the track and calorimeter isolation cones around the photon. To estimate these efficiencies, we use the data-like MCDP and MCDI samples described in Section IV.

Using these models, we find the ratio of the geometric and kinematic acceptances for DP and DI events to be $A_{DP}/A_{DI} = 0.551 \pm 0.010$ (stat) ± 0.030 (syst) for the inclusive sample and $A_{DP}^{\text{HF}}/A_{DI}^{\text{HF}} = 0.567 \pm 0.021$ (stat) ± 0.052 (syst) for the HF sample. The difference between the A_{DP} and A_{DI} acceptances is caused by an average difference of 0.5 GeV in jet p_T due to the offset energy entering the jet cone from the second vertex [30]. This significantly increases the reconstruction efficiency of jets (mainly for second and third jets) in DI events. The differences between the acceptances obtained with data-like and default MCDP and MCDI models are taken as systematic uncertainty. An additional systematic uncertainty (about 1%) is caused by the difference between

photon identification efficiencies obtained with SHERPA and PYTHIA. For the HF sample, we also correct for the b -tagging selection efficiency. The ratio of the HF jet selection efficiencies is $\varepsilon_{DP}^{\text{HF}}/\varepsilon_{DI}^{\text{HF}} = 1.085 \pm 0.019$. This number is obtained by weighting b - and c -jet efficiencies with their fractions found in Section VII A. The typical HF jet selection efficiency is 60% (10%) for the tight $b(c)$ jet selection. Only about 0.5% of the light jets are misidentified as heavy flavor jets [20, 31]. The b -tagging efficiency decreases with increasing number of $p\bar{p}$ collision vertices due to a larger hit density in the SMT detector and a decrease in the track reconstruction efficiency. This also explains the lower $N_{2\text{vtx}}/N_{1\text{vtx}}$ ratio for the HF sample compared to the inclusive sample in Table II.

C. Vertex efficiencies

The vertex efficiency $\varepsilon_{1\text{vtx}}$ ($\varepsilon_{2\text{vtx}}$) corrects for single (double) collision events that are lost in the DP (DI) candidate sample because of the single (double) vertex requirements ($|z_{\text{vtx}}| < 60$ cm and ≥ 3 tracks). The ratio $\varepsilon_{1\text{vtx}}/\varepsilon_{2\text{vtx}}$ is calculated from the data and found to be 1.05 ± 0.01 . The probability to miss a hard interaction event having at least one jet with $p_T > 15$ GeV due to a non-reconstructed vertex is $< 0.5\%$ and is ignored.

We might also have an additional fake reconstructed vertex that passes the vertex requirement. This probability is estimated using $\gamma + \text{jet}$ events and $\gamma + \geq 3$ jet events simulated in MC without zero-bias events overlay, as these events should contain only one vertex. We find that the probability to have a second (fake) vertex is $< 0.1\%$ and is ignored.

D. Calculating R_c , σ_{hard} , $N_{1\text{coll}}$ and $N_{2\text{coll}}$

We calculate the numbers of expected events with one ($N_{1\text{coll}}$) and two ($N_{2\text{coll}}$) $p\bar{p}$ collisions resulting in hard interactions following the procedure of Ref. [15], which uses the hard $p\bar{p}$ interaction cross section $\sigma_{\text{hard}} = 44.76 \pm 2.89$ mb. The values of $N_{1\text{coll}}$ and $N_{2\text{coll}}$ are obtained from a Poisson distribution parametrized with the average number of hard interactions in each bin of the instantaneous luminosity L_{inst} distribution, $\langle n \rangle = (L_{\text{inst}}/f_{\text{cross}})\sigma_{\text{hard}}$, where f_{cross} is the frequency of beam crossings for the Tevatron [23]. Summing over all L_{inst} bins, weighted with their fractions, we get $R_c = (1/2)(N_{1\text{coll}}/N_{2\text{coll}})(\varepsilon_{1\text{vtx}}/\varepsilon_{2\text{vtx}}) = 0.45$. This number is smaller by approximately a factor of two compared to that for the data collected earlier as reported in Ref. [15]. Since R_c and σ_{hard} enter Eq. 5 for σ_{eff} as a product, any increase of σ_{hard} leads to an increase of $\langle n \rangle$ and, as a consequence, to a decrease in R_c , and vice versa. Due to this partial cancellation of uncertainties, although the measured value of σ_{hard} has a 6% relative uncertainty, the product $R_c\sigma_{\text{hard}}$ only has a 2.6% uncertainty, $R_c\sigma_{\text{hard}} = 18.92 \pm 0.49$ mb.

VIII. RESULTS

Using Eq. 5, we obtain the following effective cross sections:

$$\sigma_{\text{eff}}^{\text{incl}} = 12.7 \pm 0.2 (\text{stat}) \pm 1.3 (\text{syst}) \text{ mb}, \quad (14)$$

$$\sigma_{\text{eff}}^{\text{HF}} = 14.6 \pm 0.6 (\text{stat}) \pm 3.2 (\text{syst}) \text{ mb}. \quad (15)$$

Within uncertainties, the effective cross section in the inclusive event sample is consistent with that in the event sample with identified heavy flavor jets.

The main sources of systematic uncertainties are summarized in Table VII. They are caused by uncertainties in the DP and DI fractions, the ratio of efficiencies and acceptances in DP and DI events (“ $\varepsilon_{\text{DP}}/\varepsilon_{\text{DI}}$ ”), signal fractions (“sig. frac.”), the uncertainty in the ratio of the number of hard interactions with single and double $p\bar{p}$ hard collisions times σ_{hard} (“ $R_c\sigma_{\text{hard}}$ ”), and jet energy scale (“JES”). The latter is obtained from the variation of JES uncertainties up and down by one standard deviation for all three jets [30].

Figure 5 shows all existing measurements of σ_{eff} . The $\sigma_{\text{eff}}^{\text{incl}}$ and $\sigma_{\text{eff}}^{\text{HF}}$ from this measurement agree both with the previous D0 measurement [15] and with those obtained by other experiments. These new measurements of σ_{eff} are the most accurate to date, and also provide the first measurement involving heavy quarks.

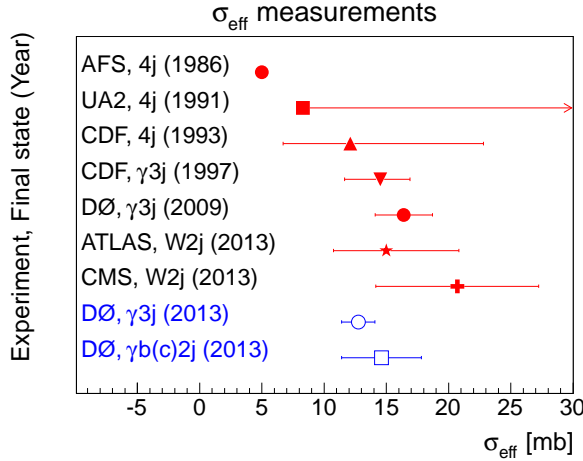


FIG. 5: (color online) Existing measurements of effective cross section, σ_{eff} , compared with result presented here (AFS: no uncertainty is reported; UA2: only a lower limit is provided).

IX. DISCUSSION OF PDF EFFECTS

The experimentally measured effective cross section σ_{eff} , presented in Eqs. 14 and 15, should be corrected for the effect of double parton PDF (dPDF) evolution [35–37]. The dPDF evolution starts at a small scale Q_0 , $\mathcal{O}(1$

GeV), where the two PDFs corresponding to partons participating in DP scattering can be factorized. The dPDF evolution results in a correlation term at a larger energy scale Q , which necessitates the following correction: $[\sigma_{\text{eff}}]^{-1} = [\sigma_{\text{eff}}^0]^{-1}(1 + \Delta(Q))$ [35], where $\Delta(Q)$ is a contribution induced by the dPDF correlation term, and σ_{eff}^0 depends only on the spatial distribution of parton flavors. To estimate this correction factor, we have employed software, provided by the authors of Ref. [36]. It uses a numerical integration of the leading order DGLAP [38] equation for the dPDFs, and which may be used to evolve the input dPDFs to any other scale. To get access to the kinematics of the first and second parton interactions, the relevant part of the PYTHIA code was modified for us by the PYTHIA authors. The evolution effect has been evaluated by examining the ratio

$$R_p(x_1, x_2; Q) = \frac{D_p(x_1, x_2; Q)}{D_p(x_1; Q)D_p(x_2; Q)} \quad (16)$$

where $D_p(x_1, x_2; Q)$ is the dPDF with the parton momentum fractions x_1, x_2 of the two partons participating in the first and second parton interactions on the proton side at scale Q , and $D_p(x_{1(2)}; Q)$ is a single parton MSTW2008LO PDF [39]. A similar equation can be written for the partons on the antiproton side. Using the simulated $\gamma + 3$ jet and $\gamma + b/c$ jet + 2 jet events, and applying our kinematic cuts, we have found the product of the two ratios $R_p R_{\bar{p}} = 1.01$ for $\gamma + 3$ jet and 1.02 for $\gamma + b/c$ jet + 2 jet events. This correction is expected to have a larger deviation from unity for higher Q (e.g., it was found to be 0.93 for $\gamma + 3$ jet at $p_T^\gamma = 70$ GeV that corresponds to the previous D0 measurement [15]). In general, it should be calculated for each set of final states and kinematic selections. Currently, the dPDF evolution implemented in Ref. [36] is available at leading order accuracy, while having it at next-to-leading order would be preferable. Due to the smallness of the found correction (1.01–1.02), and uncertainties related with the leading order approximation, this correction is not applied to the measured σ_{eff} .

X. SUMMARY

We have analyzed samples of $\gamma + 3$ jet and $\gamma + b/c$ jet + 2 jet events collected by the D0 experiment with an integrated luminosity of about 8.7 fb^{-1} and determined the fractions of events with hard double parton scattering occurring in a single $p\bar{p}$ collision at $\sqrt{s} = 1.96 \text{ TeV}$. In the kinematic region $p_T^\gamma > 26 \text{ GeV}$, $p_T^{\text{jet1}} > 15 \text{ GeV}$, $15 < p_T^{\text{jet2,3}} < 35 \text{ GeV}$, we observe that about $(21 \pm 1)\%$ and $(17 \pm 2)\%$ of the events are produced in double parton interactions in the $\gamma + 3$ jet and $\gamma + b/c$ jet + 2 jet final states. The effective cross section σ_{eff} , which characterizes the spatial transverse parton distribution in a nucleon, is found to be $\sigma_{\text{eff}}^{\text{incl}} = 12.7 \pm 0.2 (\text{stat}) \pm 1.3 (\text{syst}) \text{ mb}$ in $\gamma + 3$ jet and $\sigma_{\text{eff}}^{\text{HF}} = 14.6 \pm 0.6 (\text{stat}) \pm 3.2 (\text{syst}) \text{ mb}$ in $\gamma + b/c$ jet + 2 jet final states.

TABLE VII: The systematic uncertainties from measurement of DP (f_{DP}) and DI (f_{DI}) fractions, the ratio of efficiencies and acceptances in DP and DI events (“ $\varepsilon_{\text{DP}}/\varepsilon_{\text{DI}}$ ”), signal fractions (“sig. frac.”), the uncertainty in the ratio of the number of hard interactions with single and double $p\bar{p}$ hard collisions times σ_{hard} (“ $R_c\sigma_{\text{hard}}$ ”), and jet energy scale (“JES”), shown together with overall systematic (δ_{syst}), statistical (δ_{stat}) and total δ_{total} uncertainties (in %) for the σ_{eff} measurement. The total uncertainty δ_{total} is calculated by adding the systematic and statistical uncertainties in quadrature.

Data	Sources of systematic uncertainty								
Sample	f_{DP}	f_{DI}	$\varepsilon_{\text{DP}}/\varepsilon_{\text{DI}}$	sig. frac.	$R_c\sigma_{\text{hard}}$	JES	δ_{syst}	δ_{stat}	δ_{total}
Inclusive	3.9	6.5	5.6	2.0	2.6	2.9	10.4	1.8	10.6
HF	11.6	11.2	9.4	10.4	2.6	1.3	21.6	4.0	22.0

Our value of σ_{eff} is in agreement with the results of previous measurements and has a higher precision. This is the first measurement of σ_{eff} with heavy flavor jets in the final state. Due to the significant dominance of the Compton-like process (see Fig. 1), we may conclude that there is no evidence for a dependence of σ_{eff} on the initial parton flavor.

Acknowledgements

We are grateful to J. R. Gaunt, W. J. Stirling, T. Sjöstrand and P. Z. Skands for providing their codes and many helpful discussions.

We thank the staffs at Fermilab and collaborating institutions, and acknowledge support from the DOE and NSF (USA); CEA and CNRS/IN2P3 (France); MON, NRC KI and RFBR (Russia); CNPq, FAPERJ, FAPESP and FUNDUNESP (Brazil); DAE and DST (India); Colciencias (Colombia); CONACyT (Mexico); NRF (Korea); FOM (The Netherlands); STFC and the Royal Society (United Kingdom); MSMT and GACR (Czech Republic); BMBF and DFG (Germany); SFI (Ireland); The Swedish Research Council (Sweden); and CAS and CNSF (China).

XI. APPENDIX

In Section VIA, we estimate the DP event fraction using the predictions of Monte Carlo SP models. In this appendix, we test variables that characterize the SP model

and are related to the ΔS distribution used to calculate the DP fractions in Section VIA.

The variable $\Delta\phi(\gamma, \text{jet1})$ is sensitive to initial and final state radiation and is strongly correlated to the p_T sum vector of the photon and leading jet system, $\vec{P}_T^1 = \vec{p}_T^\gamma + \vec{p}_T^{\text{jet1}}$ (see Eq. 6). We compare the distribution of $\Delta\phi(\gamma, \text{jet1})$ in the MC SP sample to data. The latter is obtained after subtracting the DP contribution, predicted by the DP data model MIXDP, according to the DP fractions in Eqs. 7 and 8.

The comparison of the $\Delta\phi(\gamma, \text{jet1})$ spectra for the SP model extracted from data with those in the SHERPA and PYTHIA MC generators is shown in Fig. 6. The SHERPA SP event model agrees better with the data compared to PYTHIA, where the $\Delta\phi(\gamma, \text{jet1})$ distribution is shifted towards π , resulting in much worse agreement with data. For this reason, the subsequent analysis is performed using the SHERPA SP model only.

The MC SP predictions for the p_T spectra of the second and third jets are also important since, in addition to the vector \vec{P}_T^1 , they form the other imbalance vector of the ΔS variable, $\vec{P}_T^2 = \vec{p}_T^{\text{jet2}} + \vec{p}_T^{\text{jet3}}$ (see Eq. 6). Figure 7 illustrates the transverse momenta of the second and third jets of the SHERPA and data SP models. Both jet- p_T spectra in SHERPA agree well with those in data.

However to construct a better (data-like) SP model, the original default SP model from SHERPA is reweighted either in $\Delta\phi(\gamma, \text{jet1})$ bins, or in two dimensions of second and third jet p_T . These two alternative data-like SP models are considered in Section VIA to calculate the DP fractions. The later are compared to the DP fractions obtained with the default SP model to derive related systematic uncertainties.

-
- [1] P.V. Landshoff and J.C. Polkinghorne, Phys. Rev. D **18**, 3344 (1978); C. Goebel, F. Halzen, and D.M. Scott, Phys. Rev. D **22**, 2789 (1980).
 - [2] F. Takagi, Phys. Rev. Lett. **43**, 1296 (1979); N. Paver and D. Treleani, Nuovo Cimento A **70**, 215 (1982).
 - [3] B. Humpert, Phys. Lett. B **131**, 461 (1983); B. Humpert and R. Odorico, Phys. Lett. B **154**, 211 (1985).
 - [4] T. Sjöstrand and M. van Zijl, Phys. Rev. D **36**, 2019 (1987).
 - [5] G. Calucci and D. Treleani, Nucl. Phys. B (Proc. Suppl.) **71**, 392 (1999); G. Calucci and D. Treleani, Phys. Rev. D **60**, 054023 (1999).
 - [6] G. Calucci and D. Treleani, Phys. Rev. D **79**, 074013 (2009).
 - [7] C. Flensburg, G. Gustafson, L. Lonnblad, and A. Ster, J. High Energy Phys. **06** (2011) 066.
 - [8] T. Sjöstrand and P. Z. Skands, J. High Energy Phys. **03** (2004) 053.
 - [9] A. M. Snigirev, Phys. Rev. D **68**, 114012 (2003); V. L. Korotkikh and A. M. Snigirev, Phys. Lett. B **594**,

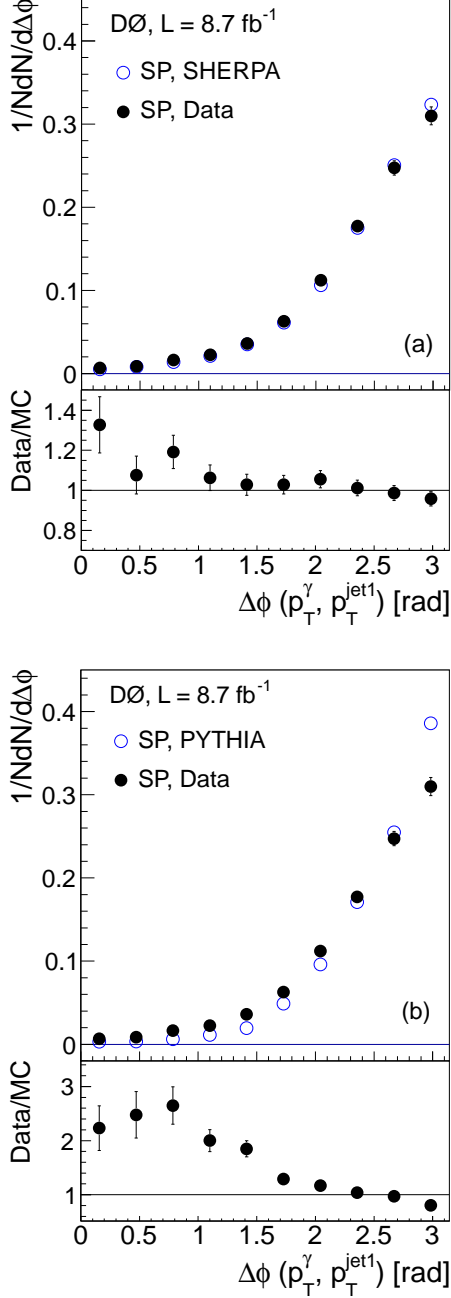


FIG. 6: (color online) The $\Delta\phi(\gamma, \text{jet1})$ distribution in the SP model extracted from data compared to that in (a) SHERPA, (b) PYTHIA. The uncertainties shown are statistical only.

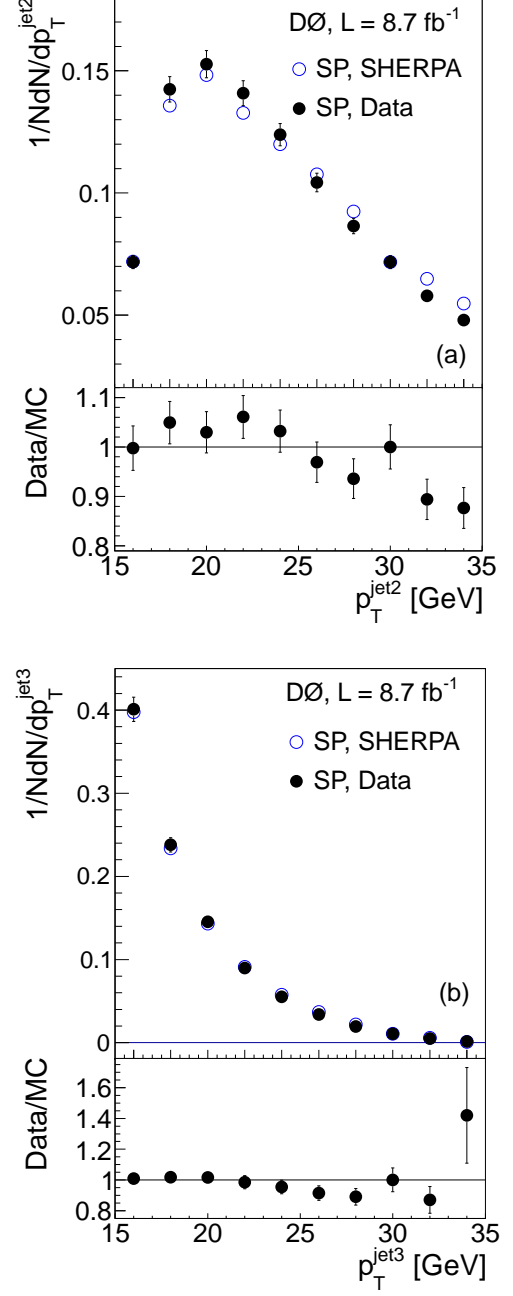


FIG. 7: (color online) Spectra of the transverse momenta of (a) second and (b) third jets in the SHERPA and data SP models. The uncertainties shown are statistical only.

- 171 (2004).
 [10] L. Frankfurt, M. Strikman, and C. Weiss, Phys. Rev. D **69**, 114010 (2004); Phys. Rev. D **83**, 054012 (2011).
 [11] T. Akesson *et al.* (AFS Collaboration), Z. Phys. C **34**, 163 (1987).
 [12] J. Alitti *et al.* (UA2 Collaboration), Phys. Lett. B **268**, 145 (1991).
 [13] F. Abe *et al.* (CDF Collaboration), Phys. Rev. D **47**, 4857 (1993).

- [14] F. Abe *et al.* (CDF Collaboration), Phys. Rev. D **56**, 3811 (1997).
 [15] V. M. Abazov *et al.* (D0 Collaboration), Phys. Rev. D **81**, 052012 (2010).
 [16] V. M. Abazov *et al.* (D0 Collaboration), Phys. Rev. D **83**, 052008 (2011).
 [17] G. Aad *et al.* (ATLAS Collaboration), New J. Phys. **15**, 033038 (2013).
 [18] S. Chatrchyan *et al.* (CMS Collaboration), submitted to

- J. High Energy Phys., arXiv:1312.5729 [hep-ex].
- [19] M. Drees and T. Han, Phys. Rev. Lett. **77**, 4142 (1996).
 - [20] V.M. Abazov *et al.* (D0 Collaboration), Phys. Lett. B **714**, 32 (2012); V.M. Abazov *et al.* (D0 Collaboration), Phys. Lett. B **719**, 354 (2013).
 - [21] T. Sjöstrand, *et al.*, J. High Energy Phys. 05 (2006) 026.
 - [22] P. Nadolsky *et al.*, Phys. Rev. D **78**, 013004 (2008).
 - [23] V. M. Abazov *et al.* (D0 Collaboration), Nucl. Instrum. Methods Phys. Res. A **565**, 463 (2006).
 - [24] M. Abolins *et al.*, Nucl. Instrum. Methods Phys. Res. A **584**, 75 (2008).
 - [25] R. Angstadt *et al.*, Nucl. Instrum. Methods Phys. Res. A **622**, 298 (2010).
 - [26] The polar angle θ and the azimuthal angle ϕ are defined with respect to the positive z axis, which is along the proton beam direction. Pseudorapidity is defined as $\eta = -\ln[\tan(\theta/2)]$. η_{det} and ϕ_{det} are the pseudorapidity and the azimuthal angle measured with respect to the center of the detector.
 - [27] V. M. Abazov *et al.* (D0 Collaboration), Phys. Rev. D **88**, 072008 (2013).
 - [28] V. M. Abazov *et al.* (D0 Collaboration), submitted to Nucl. Instrum. Methods Phys. Res. Sect. A, arXiv:1401.0029 [hep-ex].
 - [29] G. C. Blazey *et al.*, arXiv:0005012 [hep-ex].
 - [30] V. M. Abazov *et al.* (D0 Collaboration), submitted to Nucl. Instrum. Methods Phys. Res. Sect. A, arXiv:1312.6873 [hep-ex].
 - [31] V. M. Abazov *et al.* (D0 Collaboration), Nucl. Instrum. Methods Phys. Res. Sect. A **620**, 490 (2010); V. M. Abazov *et al.* (D0 Collaboration), submitted to Nucl. Instrum. Methods Phys. Res. Sect. A, arXiv:1312.7623 [hep-ex].
 - [32] T. Gleisberg *et al.*, J. High Energy Phys. 02 (2009) 007.
 - [33] S. Agostinelli *et al.*, Nucl. Instrum. Methods Phys. Res. A **506**, 3 (2003).
 - [34] R. Barlow and C. Beeston, Comp. Phys. Comm. **77**, 219 (1993).
 - [35] A.M. Snigirev, Phys. Rev. D **81**, 065014 (2010).
 - [36] J. R. Gaunt and W. J. Stirling, J. High Energy Phys. 03 (2010) 005.
 - [37] V. L. Korotkikh and A. M. Snigirev, Phys. Lett. B **594**, 171 (2004).
 - [38] V. N. Gribov and L.N. Lipatov, Sov. J. Nucl. Phys. **15**, 438 (1972); **15**, 675 (1972); L. N. Lipatov, Sov. J. Nucl. Phys. **20**, 94 (1974); Yu. L. Dokshitzer, Sov. Phys. JETP **46**, 641 (1977); G. Altarelli and G. Parisi, Nucl. Phys. B **126**, 298 (1977).
 - [39] A. D. Martin *et al.*, Eur. Phys. J. C **63**, 189 (2009).